In crystallo thermodynamic analysis of conformational change of the topaquinone cofactor in bacterial copper amine oxidase

Takeshi Murakawa[a,1], Seiki Baba[b,1], Yoshiaki Kawano[c], Hideyuki Hayashi[d], Takato Yano[a], Takashi Kumasaka[b], Masaki Yamamoto[c], Katsuyuki Tanizawa[e], and Toshihide Okajima[d,e,2]

[a]Department of Biochemistry, Osaka Medical College, Takatsuki, 569-8686 Osaka, Japan; [b]Protein Crystal Analysis Division, Structure Analysis Promotion Group, Japan Synchrotron Radiation Research Institute, Sayo-gun, 679-5198 Hyogo, Japan; [c]Advanced Photon Technology Division, RIKEN SPring-8 Center, Sayo-gun, 679-5148 Hyogo, Japan; [d]Department of Chemistry, Osaka Medical College, Takatsuki, 569-8686 Osaka, Japan; and [e]Department of Biomolecular Science and Reaction, Institute of Scientific and Industrial Research, Osaka University, Ibaraki, 567-0047 Osaka, Japan

Edited by James S. Fraser, University of California, San Francisco, CA, and accepted by Editorial Board Member Susan Marqusee November 16, 2018 (received for review July 10, 2018)

In the catalytic reaction of copper amine oxidase, the protein-derived redox cofactor topaquinone (TPQ) is reduced by an amine substrate to an aminoresorcinol form (TPQ_{amr}), which is in equilibrium with a semiquinone radical (TPQ_{sq}). The transition from TPQ_{amr} to TPQ_{sq} is an endothermic process, accompanied by a significant conformational change of the cofactor. We employed the humid air and glue-coating (HAG) method to capture the equilibrium mixture of TPQ_{amr} and TPQ_{sq} in noncryocooled crystals of the enzyme from *Arthrobacter globiformis* and found that the equilibrium shifts more toward TPQ_{sq} in crystals than in solution. Thermodynamic analyses of the temperature-dependent equilibrium also revealed that the transition to TPQ_{sq} is entropy-driven both in crystals and in solution, giving the thermodynamic parameters that led to experimental determination of the crystal packing effect. Furthermore, we demonstrate that the binding of product aldehyde to the hydrophobic pocket in the active site produces various equilibrium states among two forms of the product Schiff-base, TPQ_{amr}, and TPQ_{sq}, in a pH-dependent manner. The temperature-controlled HAG method provides a technique for thermodynamic analysis of conformational changes occurring in protein crystals that are hardly scrutinized by conventional cryogenic X-ray crystallography.

copper amine oxidase | conformational change | crystal structure | thermodynamic analysis

Copper amine oxidases (EC 1.4.3.6, CuAOs) catalyze the oxidative deamination of various primary amines to produce the corresponding aldehydes, hydrogen peroxide, and ammonia through a ping-pong mechanism comprising two half-reactions (Fig. 1*A*) (1, 2). All CuAOs so far characterized structurally are the homodimers of a 70–95-kDa subunit, each containing a Cu^{2+} ion and a protein-derived quinone cofactor, topaquinone (TPQ) (3). We have determined X-ray crystal structures of the enzyme from *Arthrobacter globiformis* (AGAO) that had been reduced with substrate under anaerobic conditions (4–8) and demonstrated that the reduced cofactor formed in the initial reductive half-reaction has two distinct conformations: a semiquinone radical form (TPQ_{sq}), in which the 4-hydroxyl group of the cofactor is ligated axially to the copper center, and an aminoresorcinol form (TPQ_{amr}), in which the cofactor has no direct contact with the copper (designated "on-copper" and "off-copper" conformations, respectively; Fig. 1*B*) (8). Previous spectrophotometric studies revealed that the equilibrium between TPQ_{sq} and TPQ_{amr} is affected significantly by temperature and pH (8, 9); at higher pH values and temperatures, the equilibrium shifts toward TPQ_{sq}, which suggests that the conformational change of TPQ is accompanied by a change in enthalpy. However, the structural basis for the pH- and temperature-dependent equilibrium remains unresolved.

In this study, we applied the humid air and glue-coating (HAG) method to thermodynamically analyze the conformational change of TPQ in noncryocooled crystals of AGAO. The HAG method was originally developed as a protein crystal-mounting method applicable to noncryogenic X-ray crystallography, in which a protein crystal is coated by water-soluble polymer and held in an air stream with controlled humidity (10). Recently, the HAG method was further improved by using N_2 gas (enabling the maintenance of anaerobic conditions) with a system for rigorously controlling the temperature and humidity around the mounted crystal and applied to the time-resolved structural study of bovine heart cytochrome *c* oxidase at 4 °C (11); the temperature control of the crystal is expected to be more accurate and direct than for the crystal enclosed in the capillary generally used in noncryogenic crystallography. By using this method throughout the procedure from the anaerobic soaking of crystals with substrate to X-ray diffraction measurement, we could visualize the equilibrium mixture of TPQ_{amr} and TPQ_{sq} in AGAO crystals under noncryogenic conditions. Importantly, rigorous temperature control of the whole process led to the development of *in crystallo* thermodynamics of conformational changes that are

Significance

This study elucidated conformational changes of the redox quinone cofactor in bacterial copper amine oxidase during the catalytic reaction. The reaction intermediates were kept in noncryocooled crystals by coating with water-soluble polymer and placing in a humid N_2 gas stream. By changing the temperature, we could collect X-ray diffraction data of the crystals that led to the structural determination of an equilibrium mixture of different states of the cofactor. Such thermodynamic analyses of conformational changes occurring in protein crystals have been very difficult, if even possible, for cryogenic X-ray crystallography. Thermodynamic parameters obtained by the *in crystallo* thermodynamic analysis are more directly linked to structural changes than those obtained by ordinary methods in solution.

Author contributions: T.M., S.B., Y.K., K.T., and T.O. designed research; T.M., S.B., Y.K., and T.O. performed research; S.B., Y.K., T.K., and M.Y. contributed new reagents/analytic tools; T.M., S.B., Y.K., H.H., T.Y., K.T., and T.O. analyzed data; and T.M., S.B., H.H., T.Y., K.T., and T.O. wrote the paper.

The authors declare no conflict of interest.

This article is a PNAS Direct Submission. J.S.F. is a guest editor invited by the Editorial Board.

Data deposition: Atomic coordinates and structure factors for 35 structures have been deposited in the Protein Data Bank (accession nos. 5ZP5–5ZP9, 5ZPA–5ZPI, 5ZOU, 5ZOW–5ZOZ, 5ZP0–5ZP4, and 5ZPJ–5ZPT).

[1]T.M. and S.B. contributed equally to this work.

[2]To whom correspondence should be addressed. Email: tokajima@sanken.osaka-u.ac.jp.

This article contains supporting information online at www.pnas.org/lookup/suppl/doi:10.1073/pnas.1811837116/-/DCSupplemental.

Published online December 18, 2018.

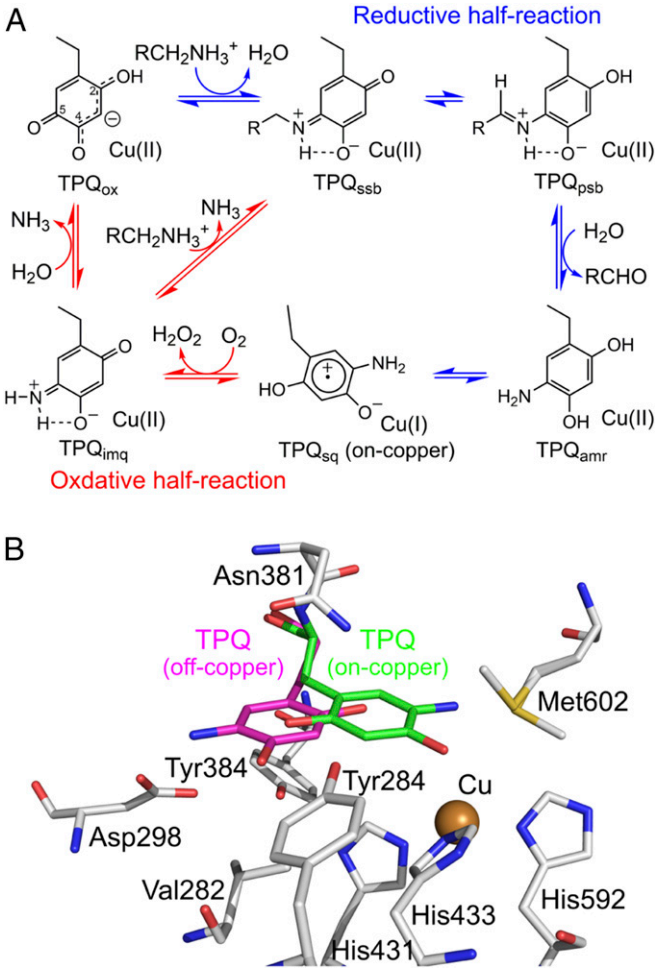

Fig. 1. Presumed catalytic mechanism and active-site structure of AGAO. (*A*) Presumed catalytic mechanism. TPQ_{ox}, oxidative form of TPQ; TPQ_{ssb}, substrate Schiff-base of TPQ; TPQ_{psb}, product Schiff-base of TPQ; TPQ_{amr}, aminoresorcinol form of TPQ; TPQ_{sq}, semiquinone radical form of TPQ; TPQ_{imq}, iminoquinone form of TPQ. (*B*) Stick model of the active site. Off-copper conformer (TPQ_{amr}) and on-copper conformer (TPQ_{sq}) are drawn in magenta and green, respectively.

observable only in noncryocooled protein crystals. Moreover, a crystal packing effect on the thermodynamic parameters can be assessed experimentally by comparison with those determined in solution.

Results and Discussion

***In crystallo* Thermodynamic Analysis for Temperature-Dependent Conformational Change.** Our previous study with AGAO crystals anaerobically reduced with a high-affinity substrate, 2-phenylethylamine (2-PEA; $K_m = 2.5$ μM) (4, 6), revealed that the oxidized product, phenylacetaldehyde (PAA), remains bound in the hydrophobic pocket close to TPQ, which could affect the TPQ_{sq}/TPQ_{amr} equilibrium (8). Therefore, we here used a low-affinity substrate, ethylamine ($K_m = 170$ mM) (6), as a reducing substrate, expecting that its oxidation product (acetaldehyde) is not bound to the pocket (8), and hence would not affect the TPQ_{sq}/TPQ_{amr} equilibrium to be investigated by X-ray crystallography, using the temperature-controlled HAG method. Diffraction data were obtained with multiple crystals selected arbitrarily from those formed in the same soaking conditions except for the temperature (4, 10, 15, and 20 °C) (*SI Appendix*, Table S1). The refined data of both of the two monomers (designated subunits A and B) contained in the asymmetric unit of AGAO crystals were included in the calculation of the averaged occupancies of TPQ intermediates (TPQ_{amr} and TPQ_{sq}). As summarized in *SI Appendix*, Table S2, the observed variance of occupancies of the assigned intermediates between the two monomers, and also among the ethylamine-reduced crystals obtained under the same conditions, is insignificant. Moreover, similar levels of *B*-factors for TPQ_{amr} and TPQ_{sq}, which are sufficiently low and comparable to those of the averaged protein *B*-factors shown in *SI Appendix*, Table S1, support the conclusion that the models are correctly accommodated in the electron density with reliable occupancies. It is also noteworthy that the similarity of *B* factors is consistent with their similar levels of the degree of disorder/mobility (thermal fluctuation). In marked contrast to the cryogenic crystallography that showed electron densities corresponding to a single conformer of TPQ (see, e.g., figs. 7 and 8 in ref. 8), those determined at four different non-cryogenic temperatures clearly showed a mixture of the two conformers (off-copper TPQ_{amr} and on-copper TPQ_{sq}) in the $F_o - F_c$ omit maps for residue 382 (TPQ; Fig. 2*A*). Relative occupancies of each conformer (*SI Appendix*, Table S2) clearly indicate that the off-copper TPQ_{amr} shifts to the on-copper TPQ_{sq} as the temperature increases (Fig. 2*B*). The occupancies of on-copper TPQ_{sq} were also consistent with the single-crystal ultraviolet–visible absorption spectra observed by the temperature-controlled HAG method, which showed that the TPQ_{sq}-specific absorption bands around 350 (shoulder), 440, and 468 nm decreased in intensity as the temperature dropped from 20 °C to 5 °C (Fig. 2*C*).

For comparison, the temperature dependence of the TPQ_{sq}/TPQ_{amr} equilibrium in the ethylamine-reduced AGAO was also studied in solution at pH 6.0. Again, absorption bands of TPQ_{sq} gradually decreased at decreasing temperatures (*SI Appendix*, Fig. S1*A*), as in crystals. The spectral change was found to be fully reversible at least in solution; reversibility of the spectral change in the crystal remains unsettled because of crystal cracking when the temperature of the blowing nitrogen gas was slowly returned from 5 °C to 20 °C after the measurement at successively decreasing temperatures in the experiment shown in Fig. 2*C*. The TPQ_{sq} content was calculated from the absorbance at 468 nm, using the extinction coefficient of TPQ_{sq} (~5,000 $M^{-1}\cdot cm^{-1}$ at 450 nm) (12). Thermodynamic parameters (Table 1) obtained from a van't Hoff plot (Fig. 2*D*) of K_{eq} values for both crystalline and solution states indicated that the significant consumption of heat ($\Delta H^\circ > 0$) in the TPQ_{amr}–TPQ_{sq} transition is mostly or excessively compensated for by a large gain of entropy ($\Delta S^\circ > 0$), resulting in a minuscule change of the free energy (ΔG°). Thus, we conclude that the TPQ_{sq}/TPQ_{amr} equilibrium is an energetically well-balanced facile process occurring both in crystals and in solution. However, we noted that the magnitude of K_{eq} (the ratio of TPQ_{sq}/TPQ_{amr}) was considerably larger in crystals than in solution at all temperatures examined (e.g., 3.6 ± 0.98 vs. 0.44 ± 0.011, respectively, at 20 °C; Fig. 2*D*).

On the basis of the modeled structure, the TPQ ring in the off-copper conformation of TPQ_{amr} is restricted in its motion, being sandwiched between the side chains of Asn381 and Tyr384/Val282 in a narrow wedge-shaped space (4) (Fig. 1*B* and *SI Appendix*, Fig. S2*A*), and tethered by a short (strong) hydrogen bond (~2.2 Å) with the side-chain hydroxyl group of Tyr284 (*SI Appendix*, Fig. S2*B*). Meanwhile, the TPQ ring of the on-copper TPQ_{sq} has sufficient freedom to rotate around the Cβ–Cγ bond (*SI Appendix*, Fig. S2*A*), even though it is tethered by a weak hydrogen bond (~3.0 Å) to the Sδ atom of Met602 (*SI Appendix*, Fig. S2*B*) (8). Thus, with regard to the rotatory movement of the TPQ ring, TPQ_{sq} has an increased mobility compared with TPQ_{amr}. Moreover, the side chains of Asn381 and Tyr384/Val282 would gain an increased mobility in the absence of the sandwiched TPQ_{amr}. Altogether, the TPQ_{sq} state should have higher entropy than the TPQ_{amr} state. These structural differences

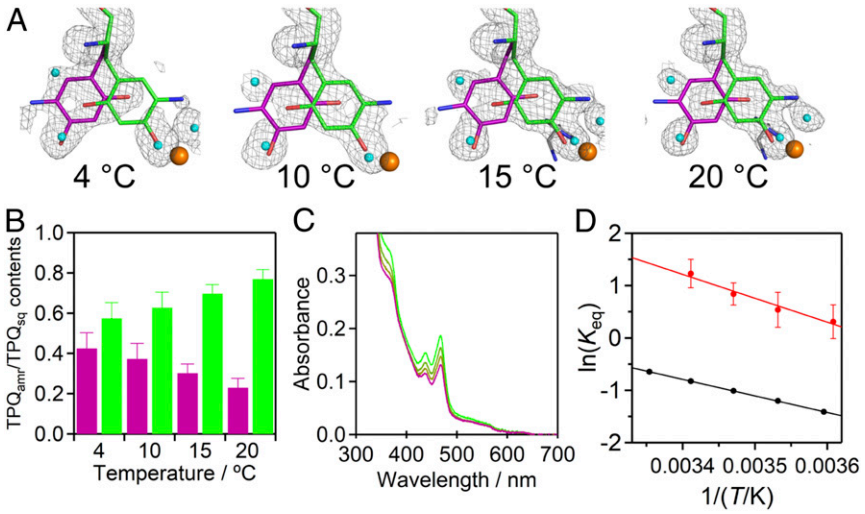

Fig. 2. Temperature dependence of TPQ_{sq}/TPQ_{amr} equilibrium. TPQ conformation in the ethylamine-reduced AGAO crystal was examined at pH 6.0, using the temperature-controlled HAG method. (*A*) Assigned models of TPQ_{sq} (green sticks) and TPQ_{amr} (magenta sticks) are superimposed on the $F_o - F_c$ omit maps (gray mesh) for residue 382 (TPQ) contoured at 3.5 σ, determined at the indicated temperatures. Water molecules and Cu atom are represented by cyan and orange spheres, respectively. Electron density maps and modeled structures at 4, 10, 15, and 20 °C were generated from datasets $AGAO_{ETA\text{-}t2}$ (subunit A of PDB entry 5ZP6), $AGAO_{ETA\text{-}t7}$ (subunit B of 5ZPB), $AGAO_{ETA\text{-}t10}$ (subunit B of 5ZPE), and $AGAO_{ETA\text{-}t14}$ (subunit B of 5ZPI), respectively (*SI Appendix*, Table S1). (*B*) Average occupancies of TPQ_{amr} and TPQ_{sq} at various temperatures are shown by magenta and green bars, respectively, with SE ($n \geq 6$), assuming that the sum of occupancies of TPQ_{amr} and TPQ_{sq} is 1.0. (*C*) Temperature-dependent change of single-crystal absorption spectra at 20, 15, 10, and 5 °C (green-to-magenta color gradation). (*D*) van't Hoff plots for the TPQ_{sq}/TPQ_{amr} equilibrium in solution and crystal. The equilibrium constants at pH 6.0 and at various temperatures were calculated from the data of *SI Appendix*, Fig. S1*B* and Fig. 2*B*: black circle, in solution; red circle, in crystal.

strongly suggest that the heat consumed during the transition to on-copper TPQ_{sq} is mainly used for breaking the strong hydrogen bond to the 4-OH group of Tyr284 in TPQ_{amr}, whereas the significant gain of entropy is a consequence of the increase in the mobility of the TPQ ring and other residues restricting the movement of TPQ_{amr}. Hence, the TPQ_{amr}–TPQ_{sq} conformational change is entropy-driven. Furthermore, the magnitudes of $\Delta H°$ and $\Delta S°$ are both ∼1.5-fold larger in crystals than in solution (Table 1). It is likely that the crystal packing leads to more energetically favorable noncovalent interactions in the crystal than in solution; this is more significant in TPQ_{amr} than in TPQ_{sq}. The ligation of TPQ_{sq} to copper anchors it in place in both crystal and solution. In contrast, TPQ_{amr} is more flexible and is more easily accommodated by the surrounding residues, leading to optimization of interactions and decrease in enthalpy and entropy of TPQ_{amr} compared with TPQ_{sq}. The packing exerts its effect on these interactions through the protein side chains and, therefore, has a more significant effect on the thermodynamic terms of TPQ_{amr}. Here, the packing leads to increased optimization of interactions and further decreases the enthalpy and entropy of TPQ_{amr}. Collectively, the crystal packing effect was experimentally and accurately evaluated from the differences in thermodynamic parameters; $\Delta\Delta H°$ ($\Delta H°_{crystal} - \Delta H°_{solution}$) = 12 kJ/mol and $\Delta\Delta S°$ ($\Delta S°_{crystal} - \Delta S°_{solution}$) = 56 (J/mol)/K.

pH Dependence of TPQ_{sq}/TPQ_{amr} Equilibrium in Crystal. We next investigated the effect of pH on the TPQ_{sq}/TPQ_{amr} equilibrium in the ethylamine-reduced AGAO crystals by the HAG method conducted at a constant temperature (15 °C) (*SI Appendix*, Table S3). Surprisingly, the occupancies of TPQ_{sq} and TPQ_{amr} were almost constant in the crystals determined at pH 6–10, showing that the equilibrium is pH-independent with nearly constant K_{eq} values of ∼3.0 (Fig. 3*A* and *SI Appendix*, Table S4). The magnitude of the TPQ_{sq}-derived absorption peak at 468 nm also did not significantly change in solution at pH 6–10 (*SI Appendix*, Fig. S3), giving an approximate K_{eq} value of 0.5 at 25 °C. These results demonstrate that the TPQ_{sq}/TPQ_{amr} equilibrium is intrinsically independent of pH both in crystals and in solution. This conclusion markedly contrasts with the previous observations that the TPQ_{sq}/TPQ_{amr} equilibrium formed in the 2-PEA–reduced enzyme is dependent on pH (in solution), involving two ionizable groups with pK_a values of 5.96 and 7.74 (*SI Appendix*, Fig. S3) (8). Thus, the pH-dependent equilibrium shift appeared to be a substrate-specific phenomenon. To identify the structural basis for the distinct pH dependences, noncryogenic structures were also determined for the 2-PEA–reduced crystals at different pH values (*SI Appendix*, Table S5). Actually, the $F_o - F_c$ omit maps for the TPQ moiety were considerably different, depending on the measured pH (Fig. 3*B* and *SI Appendix*, Table S6). In addition to the off-copper TPQ_{amr} observed at pH 8.0 and on-copper TPQ_{sq} observed at pH 8.0–10.0, two forms of a product Schiff-base of TPQ (TPQ_{psb}), which differed in configuration with regard to the Schiff-base double bond (*cis* or *trans*) (*SI Appendix*, Fig. S4), were assigned for the $F_o - F_c$ omit maps. *cis*-TPQ_{psb} assigned with 100% occupancy at pH 6.0 was probably formed by a condensation reaction between the aldehyde group of PAA that remains bound in the substrate-binding hydrophobic pocket and the 5-NH_2 group of TPQ_{amr}, as reported previously (8). At pH 7.0, the omit map was consistent with a mixture of *cis*-TPQ_{psb} with ∼55% occupancy and another TPQ_{psb} in *trans* configuration with ∼45% occupancy, which is similar, but slightly different in conformation, to the phenyl ring moiety from *trans*-TPQ_{psb} formed during the reductive half-reaction (Fig. 1*A*) (4–8). This *trans*-TPQ_{psb} was also probably formed from the bound PAA and TPQ_{amr}, suggesting that the aldehyde group of the bound PAA has a relatively unrestricted conformation at a noncryogenic temperature, as described here, so that the nucleophilic attack by the 5-NH_2 group of TPQ_{amr} is allowed from either the

Table 1. Thermodynamic parameters of equilibrium between TPQ_{amr} and TPQ_{sq}

State	In solution at pH 6.0	In crystal at pH 6.0
K_{eq}*	0.44 ± 0.011	3.6 ± 0.98
$\Delta G°$, kJ/mol†	2.0 ± 0.26	−3.0 ± 0.66
$\Delta H°$, kJ/mol‡	26 ± 0.18	38 ± 5.2
$\Delta S°$, (J/mol)/K‡	83 ± 0.62	139 ± 18
$T\Delta S°$, kJ/mol§	24 ± 0.18	41 ± 5.3

*Estimated from ε_{450} of 5,000 $M^{-1}\cdot cm^{-1}$ for TPQ_{sq} (12) or average occupancies in the crystal structures for TPQ_{sq} using the equation: $\ln K_{eq} = -(\Delta H°/RT) + \Delta S°/R$, where $\Delta H°$ and $\Delta S°$ represent the standard enthalpy and entropy changes, respectively, and R and T are gas constant and absolute temperature, respectively. The values are at 20 °C.
†Calculated using the equation: $\Delta G° = \Delta H° - T\Delta S°$ (in solution) or from K_{eq} (in crystal). The values are at 20 °C.
‡Calculated from the van't Hoff plot (Fig. 2*D*).
§The values are at 20 °C.

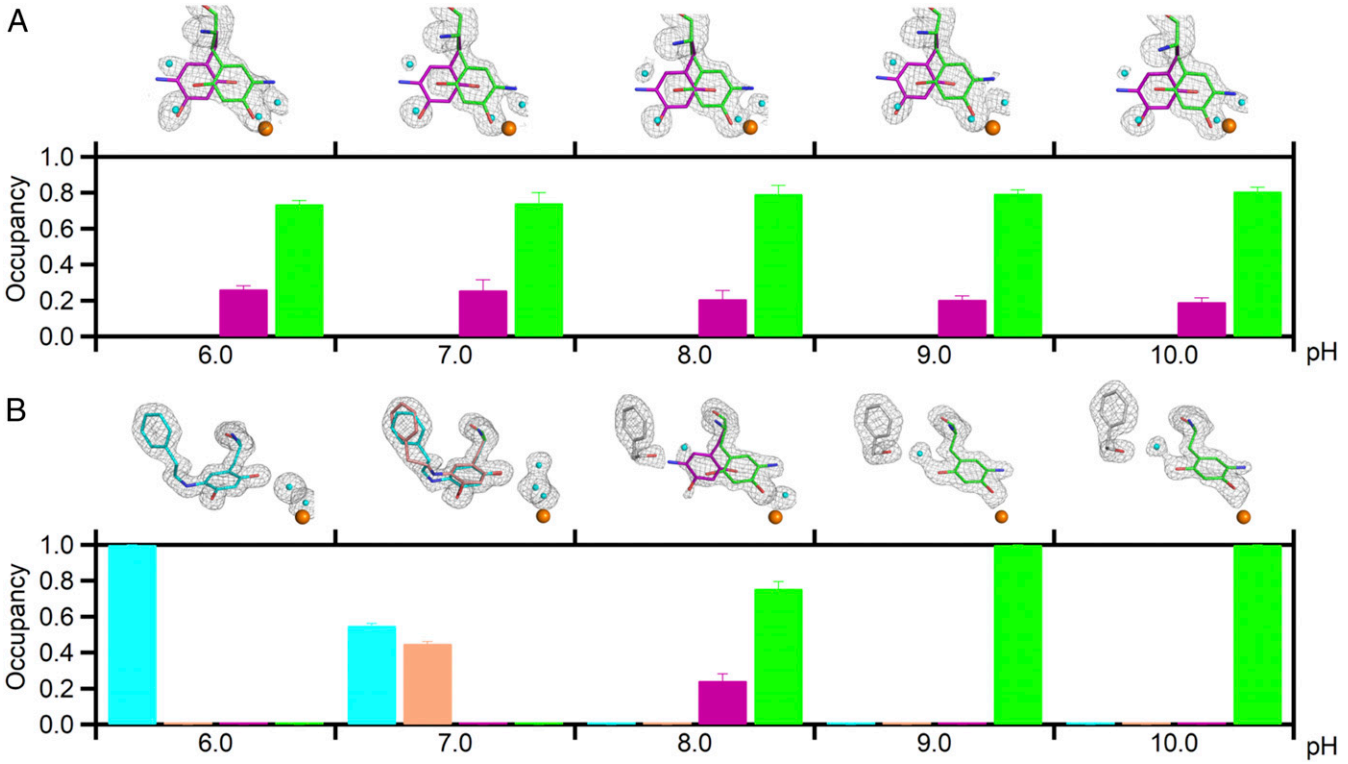

Fig. 3. pH profile of (*A*) ethylamine- and (*B*) 2-PEA–reduced crystal structures. The determined active-site structures are shown superimposed on the $F_o - F_c$ omit map (gray mesh) for residue 382 and the product aldehyde contoured at 3.5 σ. Electron density maps and modeled structures at pH 6.0, 7.0, 8.0, 9.0, and 10.0 in *A* were generated from datasets $AGAO_{ETA\text{-}p2}$ (subunit B of PDB entry 5ZOW), $AGAO_{ETA\text{-}p4}$ (subunit B of 5ZOY), $AGAO_{ETA\text{-}p6}$ (subunit B of 5ZP0), $AGAO_{ETA\text{-}p8}$ (subunit A of 5ZP2), and $AGAO_{ETA\text{-}p10}$ (subunit B of 5ZP4), respectively (*SI Appendix*, Table S3). Electron density maps and modeled structures at pH 6.0, 7.0, 8.0, 9.0, and 10.0 in *B* were generated from datasets $AGAO_{PEA2}$ (subunit A of 5ZPK), $AGAO_{PEA4}$ (subunit A of 5ZPM), $AGAO_{PEA5}$ (subunit A of 5ZPN), $AGAO_{PEA9}$ (subunit B of 5ZPR), and $AGAO_{PEA11}$ (subunit A of 5ZPT), respectively (*SI Appendix*, Table S5). Residue 382 is represented by a stick model with the same color as in the bar graph. Water molecules and the Cu centers are represented by cyan and orange spheres, respectively. Average occupancies of the intermediates are shown by bars with SE ($n \geq 4$): cyan, *cis*-TPQ_{psb}; brown, *trans*-TPQ_{psb}; purple, TPQ_{amr}; green, TPQ_{sq}.

Si or the *Re* face of the carbonyl carbon of PAA with different conformations to form *cis*- or *trans*-TPQ_{psb}, respectively (*SI Appendix*, Fig. S4 *A* and *B*; see following for details). At pH 8.0–10.0, an isolated electron density assignable to PAA was observed. At pH 8.0, the occupancy of TPQ_{sq} was 76%, and at pH 9.0 and 10.0, TPQ_{sq} was detected exclusively (Fig. 3*B*). In contrast, in the ethylamine-reduced structures having the empty hydrophobic pocket, both TPQ_{sq} and TPQ_{amr} were constantly detected with occupancies of 79–81% and 19–21%, respectively, at pH 8.0–10.0 (Fig. 3*A*). This difference suggests that the binding of PAA to the hydrophobic pocket facilitates the transition to TPQ_{sq} at pH 9.0 and 10.0. Altogether, these results reconfirm that the TPQ_{sq}/TPQ_{amr} equilibrium is dependent on pH in the 2-PEA–reduced crystals and demonstrate that the pH dependence is derived from PAA bound in the hydrophobic pocket.

It is conceivable that the hydrophobicity introduced by the aromatic ring of the bound PAA could be a primary driving force for the TPQ_{amr}–TPQ_{sq} transition in the 2-PEA–reduced crystals at pH > 8. The short hydrogen bond between Tyr284 and TPQ_{amr} suggests a strongly polar interaction, in which the proton is shared and is disfavored in a hydrophobic environment. As the proton concentration drops, Tyr284 retains a proton and becomes more neutral, and TPQ_{amr} deprotonates to undergo a conformational change to the on-copper position so that it is away from the hydrophobic PAA. As a consequence of disruption of this polar interaction at pH 8–10, the energetically unfavorable charge would be relieved from the hydrophobic microenvironment.

A possible mechanism for the pH-dependent formation of *cis*-TPQ_{psb} and *trans*-TPQ_{psb} at pH ∼7 and below is schematically shown in Fig. 4, in which the reductive half-reaction from the initial oxidized form of TPQ (TPQ_{ox}) to TPQ_{sq} is depicted at the center and the formations of *trans*-TPQ_{psb} and *cis*-TPQ_{psb} are on the left and right sides, respectively. Both *trans*-TPQ_{psb} and *cis*-TPQ_{psb} are considered to be protonated and have one more proton than TPQ_{amr}. Thus, the two forms of TPQ_{psb} become more stable relative to TPQ_{amr} with decreasing pH. We assume involvement of the active-site base, Asp298, having an unusual pK_a (7.5 at 30 °C) (4), in the pH dependence. Our previous study demonstrated that Asp298 participates in the α-H abstraction from substrate amine, as well as in the hydrolysis of TPQ_{psb} in the reductive half-reaction (4). In the noncryogenic structure determined at pH 6.0 and 7.0, the carboxyl group of Asp298 was located close (2.8–3.4 Å away) to the imine group of TPQ_{psb}. At an alkaline pH (>8), the deprotonated carboxyl group of Asp298 would promote the attack of a water molecule on the imine carbon atom of *trans*-TPQ_{psb} and *cis*-TPQ_{psb}, and hence cause the hydrolysis of TPQ_{psb} (Fig. 4) (4). These factors account for the fact that the TPQ_{psb} structures are observed only at pH ≤ 7 (Fig. 3*B*). In addition, the protonated carboxyl group of Asp298 (major species at pH < 7.5) can form a hydrogen bond with the carbonyl O atom of PAA, with Asp298 being the hydrogen donor. This hydrogen bond fixes the aldehyde group of PAA so that its *Si* face is attacked by the amino group of TPQ_{amr}, resulting in the formation of *cis*-TPQ_{psb} (Fig. 4, *Right* and *SI Appendix*, Fig. S4*B*). In contrast, the hydrogen bond cannot be formed between the deprotonated carboxyl group of Asp298 and the carbonyl O

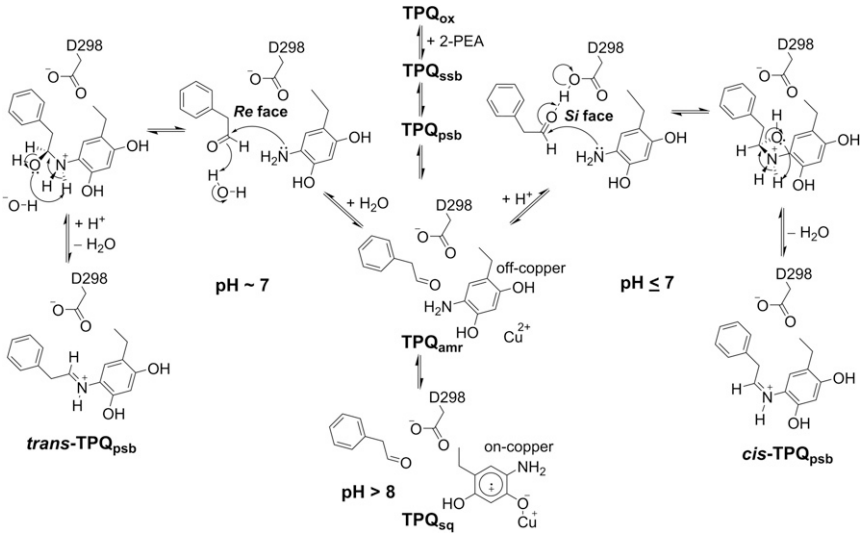

Fig. 4. Possible mechanism of pH-dependent equilibrium changes in the 2-PEA–reduced AGAO crystal.

atom of PAA. In this case, PAA could adopt a conformation in which the *Re* face is attacked by the amino group of TPQ_{amr} (*SI Appendix*, Fig. S4*A*), resulting in the formation of *trans*-TPQ_{psb} (Fig. 4, *Left*). Presumably, the aldehyde group of the bound PAA has a relatively unrestricted conformation at a noncryogenic temperature compared with the aromatic ring tightly bound at the hydrophobic pocket. In fact, the $F_o - F_c$ omit map observed at an elevated contoured level (8 σ) indicates that the aldehyde group of PAA shows considerably lower electron density than the aromatic ring and the surrounding residues such as Asp298 (*SI Appendix*, Fig. S4*C*). With Asp298 far from the carbonyl group (*SI Appendix*, Fig. S4*A*), it is most likely that a water molecule would participate in the condensation as a proton donor (Fig. 4). Considering the pK_a value of Asp298, its carboxyl group is mostly protonated at pH lower than 6, which favors the formation of *cis*-TPQ_{psb}. Only at pH 7 in the series of experiments shown in Fig. 3*B*, the deprotonated form of Asp298 could occupy a significant fraction that brings about a detectable amount of *trans*-TPQ_{psb}. Altogether, our findings suggest that the protonation/deprotonation state of Asp298 affects the reactivity of PAA with TPQ_{amr} or the lability of TPQ_{psb} to hydrolysis, generating the pH-dependent equilibrium among TPQ_{psb}, TPQ_{amr}, and TPQ_{sq}. Through the condensation with the bound PAA, TPQ_{amr} with the off-copper conformation is converted to TPQ_{psb} by protonated Asp298 at pH 6 and 7. Thus, the formation of TPQ_{psb} could be a secondary (indirect) factor for the pH dependency of the TPQ_{amr}–TPQ_{sq} transition in the 2-PEA–reduced crystals.

Conclusions

We demonstrated in this study that the temperature-controlled HAG method is useful for detecting the equilibrium mixture of the two catalytic intermediates, TPQ_{amr} and TPQ_{sq}, in AGAO crystals under noncryogenic conditions. Moreover, the HAG method is applicable to thermodynamic analyses of conformational changes occurring in protein crystals that are difficult to study by conventional cryogenic X-ray crystallography (13, 14). Importantly, thermodynamic parameters obtained by the *in crystallo* thermodynamic analysis are more directly linked to the structural changes of interest than those obtained by the ordinary methods in solution, such as spectroscopic and calorimetric analyses. Concerning the applicability of the HAG method, it should be noted that the method is limited to the conformational changes that do not lead to crystal cracking, as has been often observed in several protein crystals when soaked with ligands (15, 16). In the present study, no crack was formed on anaerobic soaking of AGAO crystals with substrate. The determined structures revealed that the conformational change is limited to the active-site region without significant global conformational changes in the main chain (4, 8).

In crystallo thermodynamic analysis in the present study showed that $\Delta H°$ and $\Delta S°$ of the TPQ_{amr}–TPQ_{sq} transition in crystal are enlarged by ∼1.5-fold compared with those in solution (Table 1). Interestingly, the increase of $\Delta H°$ and $\Delta S°$ ascribed to the packing effect is comparable to the effect of polyethyleneglycol or dextran-generating circumstances mimicking a physiological macromolecular crowding state of the cell interior (17). The environments of proteins in noncryocooled crystals might resemble those within the cell interior, such as the cytosol. This similarity suggests that the conformational changes and thermodynamic parameters determined by the temperature-controlled HAG method in the noncryocooled crystals reflect those under physiological conditions.

Various techniques of time-resolved crystallography, including the serial femtosecond crystallography with X-ray free electron laser under noncryogenic conditions, are now available to visualize motions in the enzyme active site (11, 18). The extreme brightness and ultrashort duration of X-ray free electron laser pulses enable the collection of diffraction data of protein crystals on the femtosecond timescale after initiation of the reaction. Although the serial femtosecond crystallography is an excellent method to monitor the conformational changes in crystal at ambient temperature, the temperature-controlled HAG method is useful to observe the structural equilibrium among states having distinct conformations under specified measurement conditions with a conventional X-ray beamline. The definition of conditions such as temperature and pH is essential for thermodynamic analyses. We expect that the temperature-controlled HAG method will provide an important addition to these techniques currently being developed.

Materials and Methods

Materials. Recombinant AGAO was purified as its inactive precursor form and converted to the Cu/TPQ-containing active form, as reported previously (19, 20). Protein and TPQ_{sq} concentrations were determined spectrophotometrically, using molar extinction coefficients of ε_{280} = 93,200 $M^{-1}\cdot cm^{-1}$ (19) and ε_{450} = 5,000 $M^{-1}\cdot cm^{-1}$ (12), respectively. Amine substrates, 2-PEA and ethylamine, were neutralized with 1 M H_2SO_4.

Spectrophotometric Measurements. To achieve fully anaerobic conditions, the enzyme and substrate solutions were kept in a vacuum-type glove box

(SGV-65V; Iuchi) filled with 99.999% (vol/vol) Ar gas for at least 2 h, as described previously (21). For the temperature dependence of TPQ_{sq} formation, absorption spectra of AGAO (final concentration, 100 μM monomer) reduced with 10 mM ethylamine were measured in 100 mM Hepes (pH 6.0) at a constant ionic strength ($I = 0.35 \pm 0.03$ M) that was adjusted with 100 mM Na_2SO_4. The mixture was transferred to a quartz cuvette with a gas-tight screw-cap, and temperature of the cell folder was changed from 25 °C to 20, 15, 10, and 5 °C, sequentially. Absorption spectra were measured using an Agilent 8453 photodiode-array spectrophotometer after 5 min preincubation at each temperature. After the measurement at 5 °C, temperature was returned to 25 °C to examine the reversibility of the spectral change.

Preparation of AGAO Crystals. AGAO was crystallized by microdialysis essentially according to the method described previously (4). Briefly, a 15 mg/mL protein solution was dialyzed in a 50-μL dialysis button at 16 °C against 1.05 M potassium-sodium tartrate in 25 mM Hepes buffer (pH 7.4). Single crystals with approximate dimensions of 0.5 × 1.0 × 0.2 mm grew in about 2 wk.

X-Ray Crystallography with the Temperature-Controlled HAG Method. X-ray diffraction data were obtained on BL38B1 at SPring-8, Hyogo, Japan, using the temperature-controlled HAG method, as follows. To examine the pH dependence of the substrate-reduced AGAO crystals, they were first preincubated for 24 h in 1.05 M potassium-sodium tartrate containing 25 mM Mes (pH 6.0), 25 mM Hepes (pH 7.0 and 8.0), 25 mM Taps (pH 9.0), or 25 mM Ches (pH 10.0) that became adequately anaerobic after being kept in the anaerobic environments. The crystals were further incubated in the same solution containing 10% (wt/vol) ethyleneglycol and 4 mM 2-PEA or 50 mM ethylamine for about 1 h until their color faded. The substrate soaking was performed on-site in an anaerobic chamber that was maintained at a constant temperature (4–20 °C). The reduced crystals were mounted to a cryoloop (LithoLoops; Protein Wave) and coated with aqueous polymer glue containing 10% (wt/vol) polyvinylalcohol (average polymerization degree, 4,500) and 10% (vol/vol) ethyleneglycol, according to the protocol of the HAG method (10). The mounted crystal was then enclosed in an O_2-impermeable plastic bag within the anaerobic chamber and brought to the diffractometer of the beamline. To keep the exposure to ambient air minimally, the crystal was set to the diffractometer under the nitrogen gas flow (5 L/min and 96% relative humidity) immediately after the bag was opened. The gas flow was controlled by a temperature-controlled humidifier at the same temperature as that of the crystal soaking. The anaerobicity of the mounted crystal was confirmed with a single-crystal microspectrophotometer (4). Finally, the crystal on the loop was subjected to diffraction data collection. Details of the temperature-controlling system are described in *SI Appendix, Supplementary Materials and Methods*.

For the data collection at BL38B1, the wavelength of the synchrotron radiation and oscillation range were 1.0 Å (12.40 keV) and 1.0°, respectively. Typically, the beam was ellipse shape with 200.0 × 100.0 μm (height × width) dimensions. A CCD detector (MX225HE; Rayonix) was used for detection. To minimize the radiation damage on the data collection under noncryogenic conditions, the X-ray beam was attenuated with a 700-μm-thick aluminum attenuator, and the beam radiation points were moved on the crystal gradually by 400 μm during the data collection. A total of 360 images were collected. The X-ray dose of the crystal was evaluated to be 4.8 kGy by RADDOSE-3D (22) (www.raddo.se), which is well below the level that causes significant damage to the crystal during data collection.

Single-Crystal Microspectrophotometry in the HAG Method. For the ethylamine-reduced single crystal mounted in the HAG method, temperature was gradually decreased from 20 °C to 5 °C under anaerobic conditions, and absorption spectra were measured at 20, 15, 10, and 5 °C, using the microspectrophotometer system as reported previously (4), which was settled in the hall close to the experimental hatch of the beamline.

Data Process and Refinements. The collected datasets were processed and scaled using HKL2000 (23). The initial phase was determined by molecular replacement with Phaser (24). The search model was based on the coordinates of the AGAO monomer (Protein Data Bank code 1IU7) after removing all water molecules and metal ions. Refinements, electron density map calculations, and assignment of solvent molecules were performed using Phenix (25). Manual rebuilding was performed using Coot (26), and water molecules and other ligands, such as metal ions, were added step-by-step to the model during the refinement process. PyMOL version 1.8 (Schrödinger, LLC) was used for figure drawings. Details and statistics pertaining to the data collection and refinement are summarized in *SI Appendix*, Tables S1, S3, and S5. Atomic coordinates and structure factors have been deposited in the Protein Data Bank with the accession codes as shown in *SI Appendix*, Tables S1, S3, and S5.

ACKNOWLEDGMENTS. This work was performed using synchrotron beamline station BL38B1 at the SPring-8 facility with approval from the Japan Synchrotron Radiation Institute (proposals no. 2014A1850, 2014B1148, 2014B1965, 2015A1065, 2015A1994, 2015B1979, 2016A1825, 2016A2522, 2016B1976, 2017A1854, 2017A2544, 2017A2562, 2017B2562, 2018A2513, 2018A2537). This work was supported by Japan Society for the Promotion of Science KAKENHI Grants 17K07317, JP26440037, and JP23770127 (to T.M.), JP15K05573 (to H.H.), and JP16KT0055 (to T.O.); the Platform Project for Supporting Drug Discovery and Life Science Research from the Japan Agency for Medical Research and Development under Grant JP18am0101070; and funding from the Network Joint Research Center for Materials and Devices.

1. MacIntire WS, Hartmann C (1993) Copper-containing amine oxidases. *Principles and Applications of Quinoproteins*, ed Davidson VL (Marcel Dekker, New York), pp 97–171.
2. Klema VJ, Wilmot CM (2012) The role of protein crystallography in defining the mechanisms of biogenesis and catalysis in copper amine oxidase. *Int J Mol Sci* 13: 5375–5405.
3. Okajima T, Tanizawa K (2009) Mechanism of TPQ biogenesis in prokaryotic copper amine oxidase. *Copper Amine Oxidases: Structures, Catalytic Mechanisms and Role in Pathophysiology*, eds Floris G, Mondovi B (CRC Press, Boca Raton, FL), pp 103–118.
4. Chiu YC, et al. (2006) Kinetic and structural studies on the catalytic role of the aspartic acid residue conserved in copper amine oxidase. *Biochemistry* 45:4105–4120.
5. Murakawa T, et al. (2006) Quantum mechanical hydrogen tunneling in bacterial copper amine oxidase reaction. *Biochem Biophys Res Commun* 342:414–423.
6. Taki M, et al. (2008) Further insight into the mechanism of stereoselective proton abstraction by bacterial copper amine oxidase. *Biochemistry* 47:7726–7733.
7. Murakawa T, et al. (2012) Structural insights into the substrate specificity of bacterial copper amine oxidase obtained by using irreversible inhibitors. *J Biochem* 151:167–178.
8. Murakawa T, et al. (2015) Probing the catalytic mechanism of copper amine oxidase from *Arthrobacter globiformis* with halide ions. *J Biol Chem* 290:23094–23109.
9. Shepard EM, Dooley DM (2006) Intramolecular electron transfer rate between active-site copper and TPQ in *Arthrobacter globiformis* amine oxidase. *J Biol Inorg Chem* 11: 1039–1048.
10. Baba S, Hoshino T, Ito L, Kumasaka T (2013) Humidity control and hydrophilic glue coating applied to mounted protein crystals improves X-ray diffraction experiments. *Acta Crystallogr D Biol Crystallogr* 69:1839–1849.
11. Shimada A, et al. (2017) A nanosecond time-resolved XFEL analysis of structural changes associated with CO release from cytochrome c oxidase. *Sci Adv* 3:e1603042.
12. Bisby RH, Johnson SA, Parker AW, Tavender SM (1999) Time-resolved resonance Raman studies of radicals from 4-aminoresorcinol as models for the active site radical intermediate in copper amine oxidases. *Laser Chem* 19:201–208.
13. Fraser JS, et al. (2011) Accessing protein conformational ensembles using room-temperature X-ray crystallography. *Proc Natl Acad Sci USA* 108:16247–16252.
14. Keedy DA, et al. (2014) Crystal cryocooling distorts conformational heterogeneity in a model Michaelis complex of DHFR. *Structure* 22:899–910.
15. Picot D, et al. (1991) The open/closed conformational equilibrium of aspartate aminotransferase. Studies in the crystalline state and with a fluorescent probe in solution. *Eur J Biochem* 196:329–341.
16. Pai EF, Sachsenheimer W, Schirmer RH, Schulz GE (1977) Substrate positions and induced-fit in crystalline adenylate kinase. *J Mol Biol* 114:37–45.
17. Senske M, et al. (2014) Protein stabilization by macromolecular crowding through enthalpy rather than entropy. *J Am Chem Soc* 136:9036–9041.
18. Mizohata E, Nakane T, Fukuda Y, Nango E, Iwata S (2018) Serial femtosecond crystallography at the SACLA: Breakthrough to dynamic structural biology. *Biophys Rev* 10:209–218.
19. Matsuzaki R, Fukui T, Sato H, Ozaki Y, Tanizawa K (1994) Generation of the topa quinone cofactor in bacterial monoamine oxidase by cupric ion-dependent autooxidation of a specific tyrosyl residue. *FEBS Lett* 351:360–364.
20. Murakawa T, et al. (2013) High-resolution crystal structure of copper amine oxidase from *Arthrobacter globiformis*: Assignment of bound diatomic molecules as O_2. *Acta Crystallogr D Biol Crystallogr* 69:2483–2494.
21. Kishishita S, et al. (2003) Role of copper ion in bacterial copper amine oxidase: Spectroscopic and crystallographic studies of metal-substituted enzymes. *J Am Chem Soc* 125:1041–1055.
22. Zeldin OB, Gerstel M, Garman EF (2013) RADDOSE-3D: Time- and space-resolved modeling of dose in macromolecular crystallography. *J Appl Cryst* 46:1225–1230.
23. Otwinowski Z, Minor W (1997) Processing of X-ray diffraction data collected in oscillation mode. *Methods Enzymol* 276:307–326.
24. McCoy AJ, et al. (2007) Phaser crystallographic software. *J Appl Cryst* 40:658–674.
25. Adams PD, et al. (2010) PHENIX: A comprehensive Python-based system for macromolecular structure solution. *Acta Crystallogr D Biol Crystallogr* 66:213–221.
26. Emsley P, Lohkamp B, Scott WG, Cowtan K (2010) Features and development of coot. *Acta Crystallogr D Biol Crystallogr* 66:486–501.